

Selective dehydration of glycerol on copper based catalysts

Chimentão, R. J.; Hirunsit, P.; Torres, C. S.; Ordoño, M. Borges; Urakawa, A.; Fierro, J. L.G.; Ruiz, D.

DOI

[10.1016/j.cattod.2020.09.031](https://doi.org/10.1016/j.cattod.2020.09.031)

Publication date

2020

Document Version

Accepted author manuscript

Published in

Catalysis Today

Citation (APA)

Chimentão, R. J., Hirunsit, P., Torres, C. S., Ordoño, M. B., Urakawa, A., Fierro, J. L. G., & Ruiz, D. (2020). Selective dehydration of glycerol on copper based catalysts. *Catalysis Today*, 367, 58-70. <https://doi.org/10.1016/j.cattod.2020.09.031>

Important note

To cite this publication, please use the final published version (if applicable).
Please check the document version above.

Copyright

Other than for strictly personal use, it is not permitted to download, forward or distribute the text or part of it, without the consent of the author(s) and/or copyright holder(s), unless the work is under an open content license such as Creative Commons.

Takedown policy

Please contact us and provide details if you believe this document breaches copyrights.
We will remove access to the work immediately and investigate your claim.

Selective dehydration of glycerol on copper based catalysts

R. J. Chimentão^{1,§,*}, P. Hirunsit^{2,§}, C. S. Torres¹, M. Borges Ordoño³, A. Urakawa^{3,4},

J.L.G. Fierro⁵, D. Ruiz¹

¹ *Universidad de Concepción, Facultad de Ciencias Químicas, Edmundo Larenas 129,
Casilla 160C, Chile*

² *National Nanotechnology Center (NANOTEC), National Science and Technology
Development Agency (NSTDA), Pathum Thani, 12120 Thailand*

³ *Institute of Chemical Research of Catalonia (ICIQ), The Barcelona Institute of Science
and Technology, Av. Països Catalans 16, 43007 Tarragona, Spain*

⁴ *Catalysis Engineering, Department of Chemical Engineering, Delft University of
Technology, Van der Maasweg 9, 2629 HZ Delft, The Netherlands*

⁵ *Institute of Catalysis and Petrochemistry (CSIC), Cantoblanco, 28049, Madrid, Spain*

§ These authors contributed equally

* Corresponding author: rchimenton@udec.cl

Phone number: +56 (041) 220-3354

Abstract

Glycerol is produced in large quantities as a byproduct of biodiesel, and among others hydroxyacetone (acetol) is an important commodity obtained from glycerol. Metallic Cu has been identified as active site for the dehydration of glycerol to hydroxyacetone and acid and metal sites are known to influence the catalytic performance.

In this study, dehydration of glycerol over 5 wt.% copper supported on γ -Al₂O₃, ZrO₂ and SiO₂ was investigated. Catalysts were characterized by N₂ physisorption, H₂-TPR, NH₃-TPD, N₂O chemisorption, XPS, XRD, FTIR of pyridine adsorption. Cu/ZrO₂ exhibited the highest hydroxyacetone yield at 20% of glycerol conversion and the highest apparent reaction rate. The superior activity of Cu/ZrO₂ was attributed to the highly acidic, both Lewis and Brønsted acidic, nature of the support and positive roles of the interfacial sites. The Weisz-Prater (WP) criterion was applied to confirm the absence of intraparticle diffusion limitations. It was assumed spherical particles and first order reaction. The WP value obtained in the worst scenario was less than 0.3 ensuring no diffusion limitation.

Complementary DFT study indicates that both glycerol and hydroxyacetone interact significantly stronger on Cu/ γ -Al₂O₃ and Cu/ZrO₂ compared to metallic Cu, suggesting that the active sites are at the interface of Cu particles and the acidic support.

Key-words: Glycerol, Dehydration, Hydroxyacetone, Copper, Catalyst

1. Introduction

Glycerol is a relevant bio-renewable compound for its increasing availability, since it is produced in large quantities as a by-product during the transesterification of ester to obtain biodiesel. The glycerol produced represents 10% of the total mass of the biodiesel production. Glycerol is a compound of great importance already in our daily lives, e.g. in food industry, due to its non-toxic nature [2], and it could become one of the most important building blocks for chemical production in the biorefinery [1]. Related to the latter, a variety of catalytic conversion routes to valorise the molecule, such as hydrogenolysis to propylene glycol [3], catalytic reforming [4], cracking for the production of olefins and light paraffins [5], oxidation towards acids (dihydroxyacetone, tartronic acid, glyceric acid) [6], oligomerization, polymerization towards glycerol monoesters [7], transesterification to monoglycerides [8], dehydration to acrolein or hydroxyacetone [9], carboxylation to glycerol carbonate [10], have been reported to date.

This work focuses on the selective dehydration of glycerol to hydroxyacetone. Hydroxyacetone is an interesting building block due to its extremely reactive multifunctional structure which contains hydroxyl and carbonyl functional groups. Particularly, it is an attractive intermediate of 1,2-propanediol (1,2-PDO) which is used for the synthesis of resins, liquid detergents, cosmetics, and pharmaceuticals and can be produced by hydrogenation of hydroxyacetone. 1,2-PDO is currently produced from fossil fuel derived propylene oxide. The catalytic process for the conversion of glycerol to 1,2-PDO requires external hydrogen supply. The use of external H_2 has a negative impact to the process. Direct dehydration of glycerol would form hydroxyacetone molecule without the need for hydrogen consumption

and under moderate conditions. Thus, the synthesis of 1,2-PDO from glycerol-derived hydroxyacetone offers a greener production method of 1,2-PDO and is one of the attractive paths for glycerol valorisation [3]. In addition, since hydroxyacetone is a highly reactive molecule, it can be used as an intermediate in organic synthesis to produce other compounds such as propionaldehyde, acetone and furan derivatives. Hydroxyacetone is a compound that lacks toxicity, which justifies its use in the textile, pharmaceutical and food industries. Furthermore, hydroxyacetone stands out as a key reagent for the production of lactic acid which has acquired significant interest since it is considered one of the 12 best molecules of the biological-based platform due to its wide potential applications in pharmaceutical and food industry or as biodegradable plastics among others [11].

Conventionally, hydroxyacetone has been synthesized by several ways: (i) reaction of bromoacetone with sodium or potassium formate (or acetate) followed by hydrolysis of the ester with methyl alcohol; (ii) direct oxidation of acetone with the Bayer-Villegier reagent [12]; (iii) dehydrogenation of aqueous propylene glycol in the presence of palladium-catalyzed hydrogen peroxide [13]; (iv) biosynthetic pathway which involves metabolically manipulated microorganisms using various substrates [14]. However, the presence of multi-step reagents in stoichiometric quantities, the low yields and the effluent disposal costs restrict the commercialization of any of these methods, thus the production of hydroxyacetone from inexpensive and often-wasted bio-glycerol is beneficial for environmental protection [9].

Sato *et al.* [15] investigated the dehydration of glycerol in the gas phase to hydroxyacetone over Ag catalysts achieving 91% conversion of glycerol with 86% selectivity to hydroxyacetone at 240°C under H₂ flow, however strong catalyst deactivation was observed. Chiu *et al.* [16] studied the conversion of glycerol in gas phase to hydroxyacetone in a high-pressure and high temperature semi-continuous reactor by reactive distillation over copper chromite catalyst. They observed 22% glycerol conversion and 70% hydroxyacetone selectivity. However, the toxicity associated to the Cr species in these catalysts and the deactivation due to coke formation requires further catalyst development. It has been reported that acidic sites have an important role in the glycerol dehydration and they can modulate the yield towards hydroxyacetone. The presence of Brønsted acid sites is reported to favor the dehydration of glycerol to acrolein, whereas Lewis acid sites promote the selective formation of hydroxyacetone [17].

Copper is recognized for its intrinsic ability to break preferentially the C-O primary bond of alcohols [18]. It is also suggested that copper oxide species act as Lewis acid sites to polarize the C-O bond of glycerol [19]. This property of copper is of vital importance for obtaining hydroxyacetone since this molecule is obtained by dehydration of any primary hydroxyl group of glycerol. The support material is known to participate directly on the selective dehydration. According to Sato *et al.* [1] the combination of an acid oxide support such as Al₂O₃ to copper effectively promotes the selectivity to hydroxyacetone in the glycerol conversion. This indicates that not only the copper species play an important role in the dehydration but the Lewis acid sites of the support are also important for the formation of hydroxyacetone. R. Mane *et al.* [9] investigated Cu-Al catalysts prepared by co-precipitation

and 24% glycerol conversion and 92% hydroxyacetone selectivity in the liquid phase were observed with an aqueous solution of 20 wt.% of glycerol, 220 °C and in a N₂ atmosphere.

In addition, P. Hirunsit *et al.* [20] have reported selectivity higher than 90% towards 1,2-PDO with copper catalysts supported on Al₂O₃. A. Bienholz *et al.* [21] reported for Cu/SiO₂ catalysts prepared by ammonia evaporation, 92% glycerol conversion and 69% selectivity to hydroxyacetone in gas phase with an aqueous solution of 40 wt.% glycerol in a H₂ atmosphere in a fixed bed reactor. It should be added that Dasari *et al.* [3] have reported that Raney copper has shown in the glycerol hydrogenolysis 69% selectivity towards 1,2-PDO with 49% conversion at 200°C and H₂ pressure of 14 atm.

The results outlined above may indicate that copper alone can catalyze glycerol dehydration and the support may facilitate copper species to be more active in the dehydration of glycerol. The present work focuses on the study of the selective dehydration of glycerol towards hydroxyacetone in aqueous phase on copper catalysts supported on materials with different nature of acid properties. Particularly in the present work it will be studied the effect of the total amount of acid sites; dispersion of copper species and the effect of three different supports (SiO₂, γ -Al₂O₃ and ZrO₂) in the selective dehydration of glycerol to hydroxyacetone.

2. Experimental

2.1 Catalyst preparation

Cu/ γ -Al₂O₃ and Cu/ZrO₂ catalysts were prepared by incipient impregnation with a 5% mass content of copper with respect to the weight of the support. The metal precursor was an aqueous solution of Cu(NO₃)₂·3H₂O. After the impregnation step, the samples were kept under hood at room temperature for 4 hours and finally dried at 120 °C for 24 hours. Once dried they were calcined in a muffle with a heating ramp of 5 °C min⁻¹ from room temperature to 400 °C for 4 hours. Cu/SiO₂ catalyst was prepared by ammonia evaporation method [22] with a mass content of 5% of copper relative to the support. Briefly 25 wt.% ammonia solution was added in an aqueous solution of Cu(NO₃)₂·3H₂O under vigorous stirring until it reached pH 12. The resulting solution was heated to 80 °C maintaining this temperature until it reached a pH of 6.0-7.0. The final product was filtered and washed with water, followed by drying at 120 °C for 24 hours. It was then calcined in a muffle furnace with a heating ramp of 5 °C min⁻¹ from room temperature to 400 °C for 4 hours. Finally, prior to the reaction the catalysts were reduced in a quartz reactor under H₂ flow at 50 mL min⁻¹ from room temperature to 400 °C with a heating ramp of 5 °C min⁻¹ and then they were kept at 400 °C for 4 hours.

2.2 Catalyst Characterization

The specific surface areas of the copper-based catalysts were measured with a Micromeritics ASAP 2010 physisorption apparatus with N₂ at 77 K. BET and BJH methods were used respectively for the calculation of the surface areas and pore characteristics (size distribution

and volume). Prior to the analysis, the samples (about 100 mg) were degassed for 4 hours at 120 °C using N₂ as a carrier gas.

X-ray powder diffraction (XRD) measurements were conducted on a Bruker X-ray diffractometer model D4 Endeavor (K α Cu, 40 kV and 20 mA) operating with 2 θ range of 20 - 90° at a scanning rate of 0.02° for 0.3 s.

FTIR spectra were collected using a FTIR-Vertex 70V instrument (Bruker) equipped with a Harrick cell TM (powder, ca. 30 mg). Prior to pyridine adsorption experiments, the samples were pre-treated at 400°C for 1 hour in hydrogen flow. The system was then cooled down to reach 150 °C under helium flow. Pyridine vapor adsorption was performed at 150 °C (30 spectra, 1 spectrum per minute). Finally, pyridine desorption was monitored for 1 hour under He flow at 150 °C from temperature ramping up (from 150 to 400 °C). Background spectra were collected before pyridine adsorption.

Temperature programmed desorption of NH₃ (NH₃-TPD) experiments were performed in a Micromeritics AutoChem II 2920 automatic equipment. Prior to the experiments, the catalysts (about 100 mg) were reduced at 400 °C for 120 min in 10% H₂/Ar at 20 mL min⁻¹, and after the reduction samples were cooled to 35 °C under the same flow. Then catalysts were treated with NH₃ (20 mL min⁻¹) for 10 min at 40 °C. Thus, the samples were treated in He flow (50 mL/min) to purge the system. Finally, the NH₃ desorption was carried out by heating the reactor with a temperature ramp of 5 °C min⁻¹ in a flow of He (20 mL min⁻¹). A trap of water, ice and NaCl salt was used. The NH₃ consumption has been determined by a thermal conductivity detector (TCD).

The amount of surface copper atoms was measured on the samples (about 100 mg) initially reduced in hydrogen flow of 50 mL min⁻¹ at 400 °C. The reduced samples were cooled in He flow (50 mL/min) to 60 °C and purged for 30 minutes. 20% N₂O/Ar gas was added for 1 hour. The selective oxidation of the copper surface to Cu₂O was performed under 20% N₂O/Ar flow (50 mL min⁻¹) at 60 °C:



The system was then cooled to room temperature in He flow (50 mL min⁻¹) to eliminate the physisorbed species of N₂O. Cu₂O_{surface} was further reduced with 5% H₂/Ar flow (50 mL min⁻¹) by raising the temperature at 5 °C min⁻¹ from room temperature to 900 °C. The H₂ consumption was followed by TCD detector.



VG Escalab 200R spectrometer equipped with a hemispherical electron analyser and an Mg K α (h ν =1253.6 eV, 1 eV=1.603 $\times 10^{-19}$ J) was employed for X-ray photoelectron spectroscopy (XPS) measurements. The X-ray source operated at 10 mA and 12 kV. The spectrometer chamber pressure during data acquisition was maintained at 1 $\times 10^{-7}$ Pa. The peaks were fitted by a non-linear least square fitting program using a properly weighted sum of Lorentzian and Gaussian component curves after background subtraction. The constant charging of the samples was corrected by referencing all energies to the Al 2p peak at 74.5 eV.

2.3 Catalytic Activity

Dehydration of glycerol was studied in a 300 mL batch reactor with a content of 60 mL of reaction mixture with an aqueous solution of 80 wt.% of glycerol, 500 mg of catalyst which corresponds to a glycerol/Cu molar ratio of 1000. The reaction was carried out for 3 hours under a constant stirring of 800 rpm and temperature of 190 °C. The reaction was performed under N₂ atmosphere.

The reaction products were analysed at different reaction time by an autosystem XL gas chromatograph equipped with an FID detector and Nukol Capillary column (30 m long, 0.53 mm internal diameter and 0.5 µm film space) with He as a carrier gas. The products were also analysed with a gas chromatograph coupled to a mass spectrometer. The glycerol conversion and product selectivity were calculated according to:

$$\text{Conversion (\%)} = \frac{(\text{moles of glycerol reacted})}{(\text{initial moles of glycerol})} \times 100 \quad (3)$$

$$\text{Product } i \text{ selectivity (\%)} = \frac{(\text{moles of } C \text{ in the product } i)}{(\text{moles of } C \text{ in the initial quantity of glycerol})} \times 100 \quad (4)$$

To ensure the absence of intra-particle diffusion resistance the Weisz-Prater (WP) parameter was calculated. According to WP criteria, if WP (ϕ) \leq 0.3 the internal diffusion resistance can be neglected for a heterogeneous reaction. Where ϕ is:

$$\phi = \frac{-r_{obs}\rho_c R_p^2}{D_e C_{AS}} \quad (5)$$

215 Where, $-r_{obs}$ = the observed rate ($\text{mol g}_{\text{cat}}^{-1} \text{s}^{-1}$), ρ_c = solid catalyst density = 2.08 g.cm^{-3} , R_p =
 216 catalyst particle radius = 0.0025 cm , C_{AS} = concentration of glycerol at catalyst surface =
 217 $0.001 \text{ mol cm}^{-3}$. D_e is the effective diffusivity of glycerol to water ($2.11 \times 10^{-5} \text{ cm}^2 \text{ s}^{-1}$) and:

$$218 \quad D_e = \frac{D_{AB} \phi \sigma}{\tau} \quad (6)$$

219 Where ϕ = porosity pellet = 0.42 , σ = constriction factor = 0.8 and τ = tortuosity = 3 [23, 24]
 220 and D_{AB} = diffusion coefficient of glycerol to water at 250°C = $1.85 \times 10^{-4} \text{ cm}^2 \text{ s}^{-1}$ calculated
 221 by Wilke-Chang Equation:

$$222 \quad D_{AB} = \frac{1.173 \times 10^{-13} (\phi M_B)^{0.5} T}{\mu V_A^{0.6}} \quad (7)$$

223 Where ϕ is the factor for solute-solvent interaction; Temperature (K); V_A = molar volume of
 224 solute at boiling point (glycerol), M_B = molecular weight of solvent (water) and μ is the
 225 solvent viscosity.

226

227 Finally $-r_{obs}$ is:

$$228 \quad -r_{obs} = \frac{n}{V \times m_{cat} \times t} \quad (8)$$

229 Where n = moles of glycerol reacted, V = volume in L, m_{cat} = catalyst weight in g and t =
 230 reaction time in minutes.

231

232 *2.4 Computational Details*

233 The Cu(111) surface model was constructed with a supercell of 4×4 containing 4 layers of
 234 metal atoms and a vacuum region $\sim 15 \text{ \AA}$. The two atomic layers from the bottom of the slab
 235 were fixed, while the top two layers were relaxed to their lowest energy configurations. The
 236 fixed layers were set to Cu bulk bond distances according to the optimized lattice constant

that was determined from bulk calculation. The slab model of γ - $\text{Al}_2\text{O}_3(110)$ surface contains thirty two Al_2O_3 molecular units and ~ 15 Å of the vacuum region. The (110) crystalline surface was chosen because it dominates in γ -alumina nanocrystallites (~ 70 -83% of total area) [25, 26]. Twelve of Al_2O_3 molecular units located in atomic layers from bottom of the slab were fixed and the rest were relaxed including the Cu_{13} cluster and adsorbates. The fixed layers were set to γ - Al_2O_3 bulk bond distances in which the γ - Al_2O_3 bulk model structure was taken from references [25, 27]. The tetragonal ZrO_2 bulk structure was applied followed the experimental observation. The slab model of most stable $\text{ZrO}_2(111)$ surface was modeled with total thirty nine molecular units and ~ 15 Å of the vacuum region excluding adsorbates. Seventeen ZrO_2 molecular units from the bottom of a slab were fixed and the rest were relaxed including Cu_{13} cluster and adsorbates. The structures of bare $\text{Cu}(111)$, Cu_{13}/γ - $\text{Al}_2\text{O}_3(110)$ and $\text{Cu}_{13}/\text{ZrO}_2(111)$ are shown in Fig. S5 of supporting information.

The initial geometries of isolated Cu_{13} cluster were modeled based on the possible M_{13} nanoparticle structures reported in previous studies [28, 29]; icosahedral (ICO), face centered cubic (FCC), hexagonal close packed (HCP), capped cubic (CC), buckled biplanar (BBP), triangular biplanar (TBP), and cage-like (CAG). The two most stable structures of isolated Cu_{13} cluster structures were found to be ICO and BBP (Fig. S4 of supporting information). Then, the optimized ICO and BBP Cu_{13} clusters were initially placed on the γ - $\text{Al}_2\text{O}_3(110)$ and $\text{ZrO}_2(111)$ surfaces with variations of location on the surfaces and orientations of the Cu_{13} clusters. The most stable structures found for $\text{Cu}_{13}/\text{Al}_2\text{O}_3(110)$ and $\text{Cu}_{13}/\text{ZrO}_2(111)$ (Fig. S5 of supporting information) were then applied for glycerol and hydroxyacetone adsorption study. The 13-atom Cu cluster model can represent small particle size (~ 1 nm) which has an average number of metal atoms in the range 11-14 atoms. The models present Cu-Cu and

Cu-support interaction. Cu₁₃ cluster were widely applied to study catalytic reaction such as CO oxidation and ammonia decomposition [30-32]. It should be noted that the copper particle size and shape can affect the reactivity as well which may be due to the variation of the amount of low coordinated defect sites. The supported metal-13 cluster on support such as γ -Al₂O₃ surface also were previously employed to study NO oxidation [33], H₂ dissociation [34], the nature of the metal-support interaction [35], and stability of clusters on support [36].

Hydroxyl are created and adsorbed on Al₂O₃ and ZrO₂ surfaces due to the adsorption of water which is a product of glycerol dehydration [25, 37]. The effect of hydroxylation on the supports were also investigated. The relationship between the hydroxyl coverage on γ -Al₂O₃(110) surface and temperature has been investigated previously by Digne *et al.*[25] Applying this relationship, the OH coverage on γ -Al₂O₃(110) surface corresponding to the experimental temperature in the range of 130-230 °C is approximately 3.0-11.8 OH nm⁻². The approximately 4.5 OH nm⁻² coverage corresponding to 4 H₂O molecules on the γ -Al₂O₃(110) and ZrO₂(111) surfaces were employed in this work. The hydroxyl group adsorption was particularly located nearby the copper cluster model in order to bring in the effect of hydroxylation on the dual roles of support and copper cluster.

The Vienna *ab initio* Simulation Program [38, 39] was employed to perform fully periodic plane-wave density functional theory (DFT) calculations. Spin-polarized DFT calculations were performed using the GGA-PBE functional [40] implemented with the Projector Augmented Wavefunction (PAW) [41, 42] method for representing the non-valence core electrons. The long-range dispersion force was included using the semi empirical dispersion potential correction method described by Grimme and coworkers [43, 44]. The plane-wave energy cutoff was optimized at 450 eV. The Gaussian broadening [45] with a smearing width

of 0.1 eV was employed. The dipole correction was included only in z direction and the surface Brillouin zone was sampled with a 2×2×1 Monkhorst-Pack k-point mesh [46] for all surface calculations. The results were checked for convergence with respect to energy cutoff and number of k-points. The convergence criterion for electronic self-consistent iteration was set to 10⁻⁷ eV and the ionic relaxation loop was limited for all forces smaller than 0.030 eV Å⁻¹ for free atoms. Bader charge analysis was performed using VASP-VTST [47–49].

3. Results

3.1 Catalyst characterization

The textural properties of the supports and copper catalysts are summarized in Table 1 and Fig. 1. Specific area (S_{BET}), pore volume (V_{pore}) and pore diameter (d_{pore}) of the catalysts decrease compared to their supports due to the introduction of copper, indicating a partial blockage of the pores. ZrO₂ and SiO₂ exhibited the smallest and the highest specific surface area, respectively.

Table 1. Textural parameters of supports and copper catalysts.

Sample	S_{BET} (m ² g ⁻¹)	V_{Pore} (cm ³ g ⁻¹)	d_{pore} (nm)
ZrO ₂	146	0.17	4.3
γ-Al ₂ O ₃	212	0.39	7.4
SiO ₂	319	0.85	10.6
5% Cu/ZrO ₂	131	0.13	4.0
5% Cu/γ-Al ₂ O ₃	181	0.34	7.5
5% Cu/SiO ₂	244	0.70	11.6

Fig. 1a shows N₂ sorption isotherms of the supports and Cu catalysts. Isotherms displayed a type-IV curves characteristic of mesoporous structure [50]. For SiO₂-based materials a H1-type hysteresis loop corresponding to uniform spherical pores from a regular matrix of pore size distribution centered at 10-12 nm (Fig. 1b) was found. For materials based on γ -Al₂O₃ and ZrO₂ a H2-type hysteresis loop and pore size distribution centered at 4 and 7 nm were found, respectively.

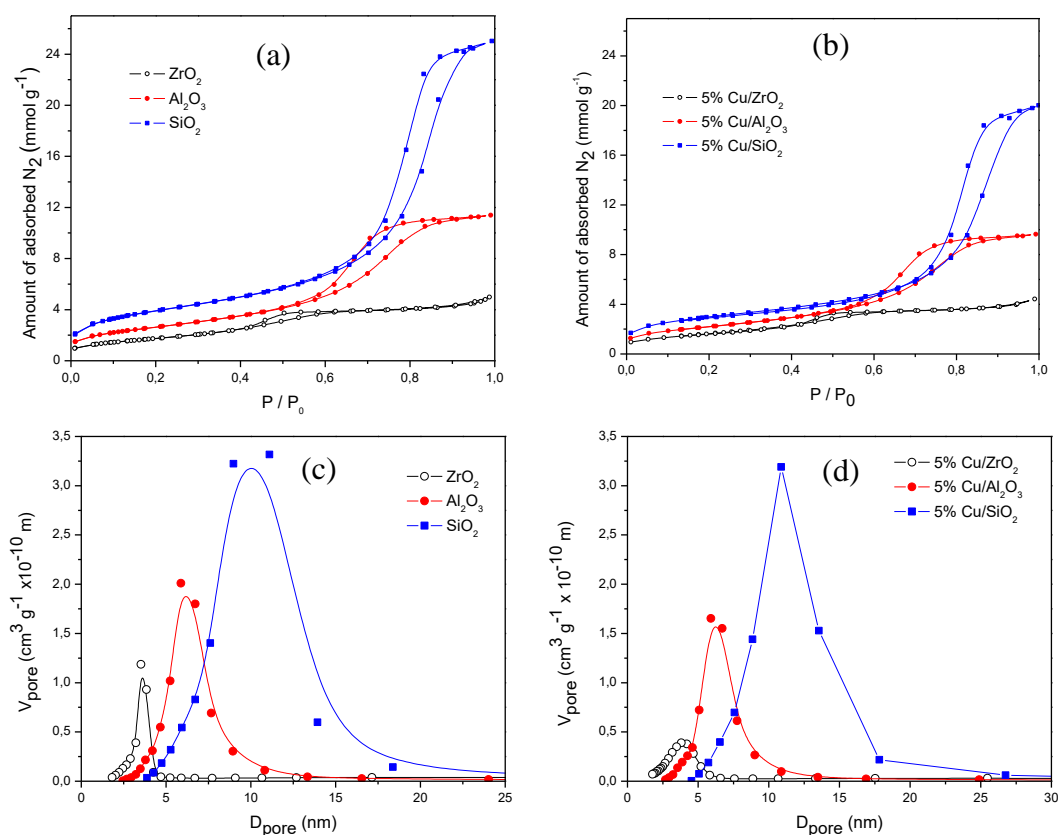


Fig. 1. (a) and (b) N₂ adsorption-desorption at 77 K and (c) and (d) Pore size distribution.

By XRD, diffraction peaks only due to the support materials (Fig. 2) were found for all samples. Copper species are expected to exhibit reflection peaks as follows: metallic copper (Cu⁰) at $2\theta = 43, 50$ and 74° (JCPDS 04-0836), copper (II) oxide (CuO) at $2\theta = 32.6, 35.6,$

38.6, 48.8, 53.6, 58.3, 61.6, 66.4, 68.1, 72.3 and 75.1 ° (JCPDS 48-1548) and copper (I) oxide (cuprous oxide, Cu₂O) at 2θ = 36.4, 42.3 and 61.3 ° (JCPDS 05-0667). The absence of the reflection peaks due to copper species indicates their high dispersion. At 7 wt.% of copper it is reported to be possible to identify Cu peaks in the XRD analysis [51]. Previous work reported that the highly crystalline CuO is formed from approximately 4 wt.% of Cu for 100 m² g⁻¹ of γ-Al₂O₃ [52].

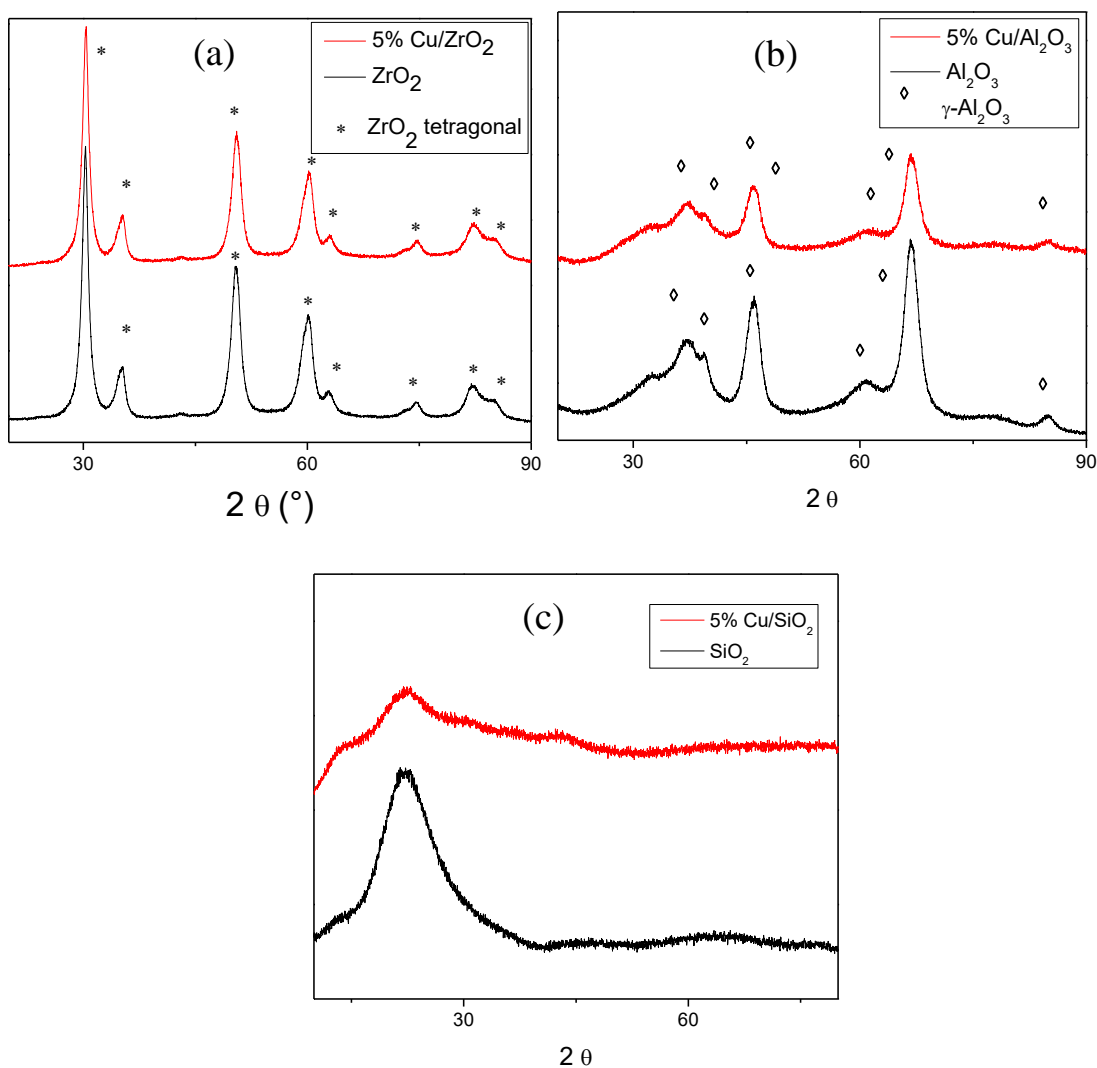


Fig. 2. Powder XRD patterns of (a) ZrO₂ (b) γ-Al₂O₃ and (c) SiO₂ materials.

Only tetragonal zirconia (no monoclinic) patterns were observed in ZrO₂-based materials (Table 2). For the materials based on γ -Al₂O₃ the presence of characteristic peaks of the support (JCPDS 029-0063) was observed at $2\theta = 31.9, 37.6, 39.5, 45.8,$ and 66.7° . X-ray diffraction reveals the amorphous nature of SiO₂.

Table 2. XRD pattern of monoclinic (JCPDS 37-1484) and tetragonal ZrO₂ (JCPDS 17-0923).

Monoclinic ZrO ₂		Tetragonal ZrO ₂	
2θ ($^\circ$)	Crystallographic plane	2θ ($^\circ$)	Crystallographic plane
24.2	(0,1,1)	30.1	(1,1,1)
28.2	(1,1,0)	35.2	(2,0,0)
31.4	(0,2,0)	50.4	(2,2,0)
34.3	(1,2,1)	59.9	(3,1,1)

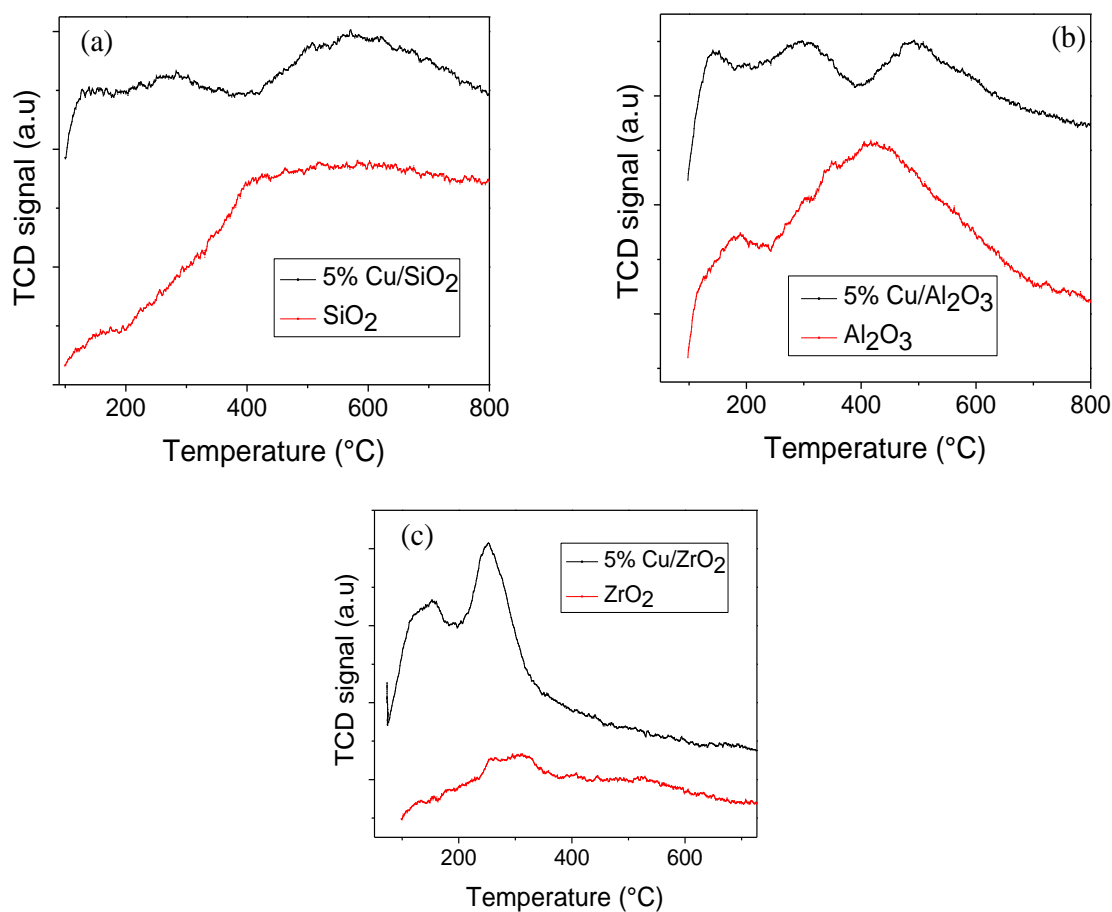
The evaluation of acidity of the support and catalyst materials by NH₃-TPD (Table 3 and Fig. 3) showed an increase of the total acidity for the catalysts containing copper species. Cu/ZrO₂ has the highest acidity ($867 \mu\text{mol g}_{\text{cat}}^{-1}$) in contrast to Cu/SiO₂ that presented the lowest total amount of acid sites ($187 \mu\text{mol g}_{\text{cat}}^{-1}$).

Table 3. Quantitative analysis of NH₃-TPD data of ZrO₂, γ -Al₂O₃ and Cu-based catalysts.

Sample	Total NH ₃ amount	
	($\mu\text{mol g}_{\text{cat}}^{-1}$)	($\mu\text{mol m}^{-2}$)
ZrO ₂	360	-----
γ -Al ₂ O ₃	280	-----
5% Cu/ZrO ₂	867	6.6
5% Cu/Al ₂ O ₃	591	3.3
5% Cu/SiO ₂	187	0.8

342

343 ZrO_2 support showed a signal with a maximum at 270 °C and a tail-like broad desorption
344 extending to approximately 630 °C, indicating a wide distribution of the strength of the acid
345 sites ranging from moderate (considered from 200-450 °C) to strong (> 450 °C) ones. The
346 Cu/ZrO_2 catalyst also exhibited a wide distribution of acid sites with different acid strengths
347 and the total amount of acid sites that increases with the introduction of copper species. This
348 could be attributed to the contribution of copper oxide species. Similarly, a heterogeneous
349 distribution of acid sites for the $\gamma\text{-Al}_2\text{O}_3$ system is highlighted. A minor or negligible total
350 amount of acid sites in the SiO_2 support was found.



351

Fig. 3. Temperature-programmed desorption of ammonia profiles of supports and Cu-based catalysts (a) SiO₂ and 5%Cu/SiO₂, (b) Al₂O₃ and 5%Cu/Al₂O₃ and (c) ZrO₂ and 5%Cu/ZrO₂.

Brönsted and Lewis acidity were identified by FTIR of pyridine as shown Fig. 4. The IR spectra of the support materials and supported copper catalysts were compared in the region of 1600-1400 cm⁻¹. From the IR spectra only Lewis acid sites were identified over the support materials. The IR spectra of the supports (γ -Al₂O₃ and ZrO₂) show bands at about 1455, 1490 and 1610 cm⁻¹ after pyridine desorption at 400 °C. The band observed at 1455 cm⁻¹ is attributed to the presence of hydrogen-bonded pyridine adsorbed on Lewis acid sites [53]. The observed band at 1610 cm⁻¹ is ascribed to pyridine strongly bound on Lewis acid sites [54]. The band observed at about 1490 cm⁻¹ is attributed to pyridine adsorbed on both Lewis and Brönsted acid sites. There is no evidence for a band at about 1610 cm⁻¹ (Fig. 4) in the infrared spectra of pyridine desorption on SiO₂. In addition, there is no evidence for a band at 1540 cm⁻¹ suggesting no Brönsted acidity for SiO₂ sample in agreement with literature [55]. It must be added that the absence of the band at 1490 cm⁻¹ suggests negligible Lewis acidity in SiO₂ support.

Supported copper catalysts were reduced at 400 °C in hydrogen prior the pyridine measurements. Impregnation of copper on ZrO₂, γ -Al₂O₃ and SiO₂ resulted in the appearance of Lewis and Brönsted acid sites. The bands corresponding to Brönsted acid sites were observed at 1548 cm⁻¹ for copper supported on γ -Al₂O₃ and ZrO₂ [56]. In contrast, Cu/SiO₂ catalyst exhibited only Lewis acid sites.

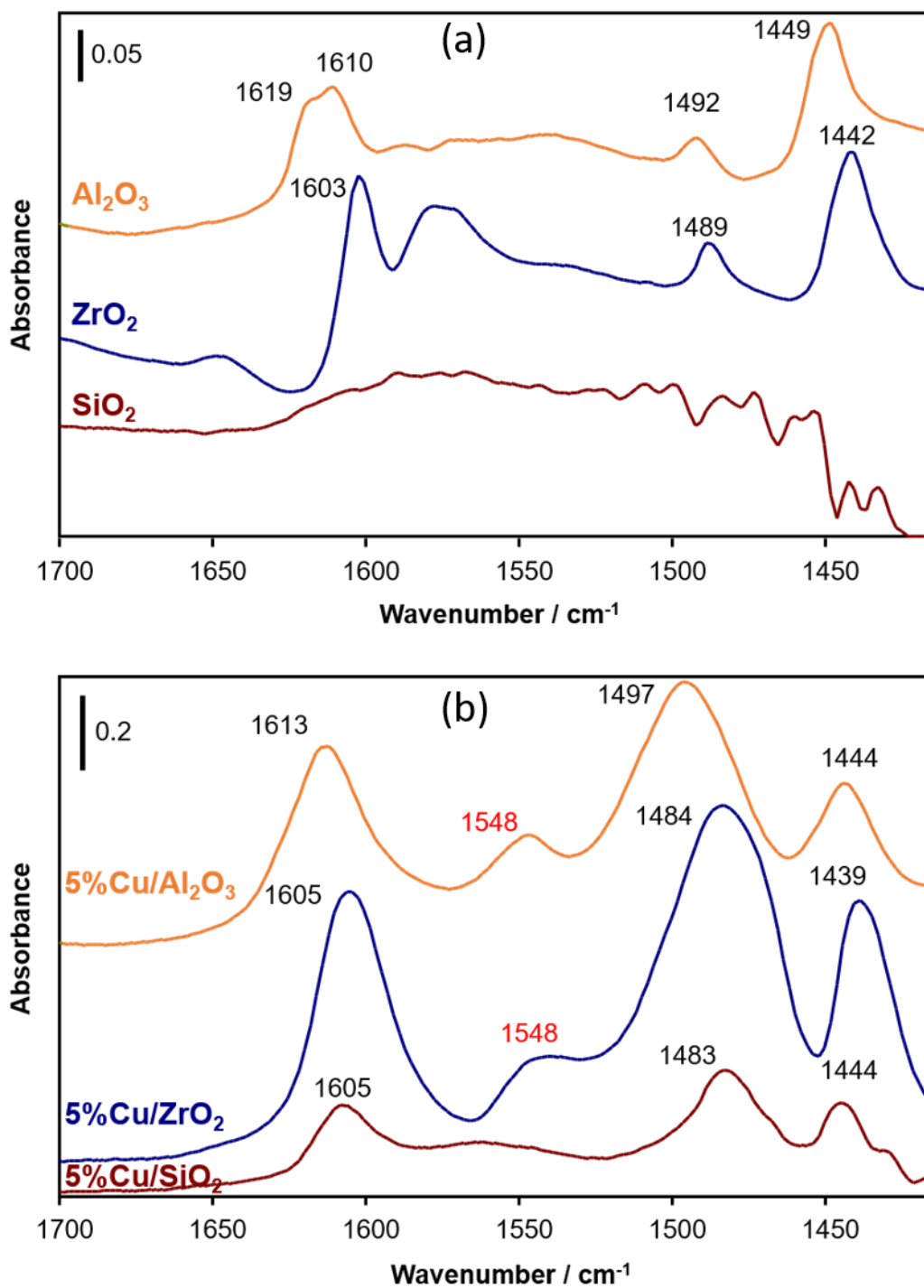


Fig. 4. FTIR of (a) supports and (b) catalyst after pyridine desorption at 400 °C.

TPR profiles of the calcined copper catalysts at 400 °C are shown in Fig. 5. Cu/SiO₂ catalyst exhibits a nearly symmetrical reduction peak at ca. 200 °C. For Cu/Al₂O₃ catalyst, the main reduction peak is also centred at ca. 200 °C. It is observed that the catalysts Cu/SiO₂ and Cu/Al₂O₃ have an reductive event at the same temperature which suggests a homogeneous copper species distribution and the corresponding reduction refers to Cu⁺²→Cu⁰ [57].

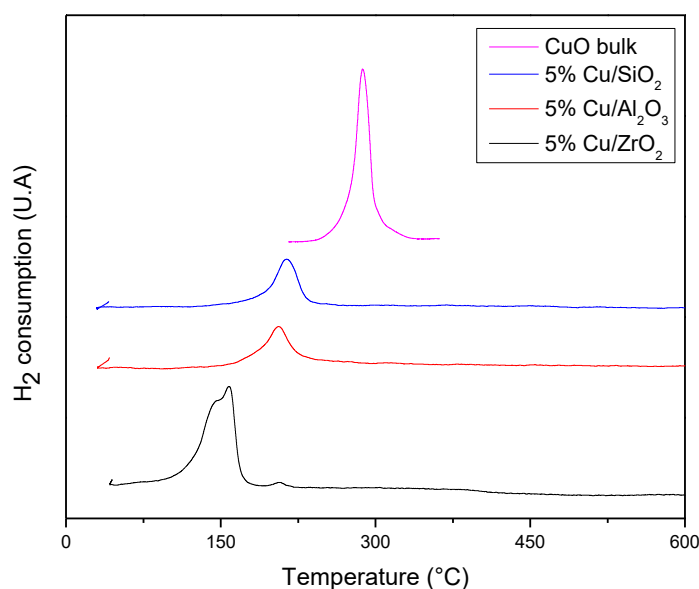


Fig. 5. TPR of copper based catalysts.

For Cu/ZrO₂ sample the main reduction peak shifts to lower temperature at ca. 160°C and presents a shoulder peak at ca. 140°C. Liu *et al.* [58] observed two overlapping peaks with apparent maxima at 140°C and 160°C for the reduction of copper supported on tetragonal zirconia. According to these authors, these peaks correspond to highly disperse Cu⁺² species assigning the first peak to the reduction of Cu⁺² → Cu⁺¹, followed by a second event to Cu⁺¹ → Cu⁰. The reduction profile of Cu/ZrO₂ sample suggests a strong influence of the support

on the reduction of copper species. A shift towards lower temperatures with respect to the other two supports (γ - Al_2O_3 and SiO_2) is observed. This is attributed to promoter effects of ZrO_2 in the reducibility of copper species. It must be added that only a minor reduction peak at 200°C was visible for Cu/ZrO_2 . This peak can be attributed to the reduction of bulk CuO [59]. The low reduction temperature strongly suggests the presence of finely dispersed copper species embedded homogeneously in the ZrO_2 support. The higher reduction temperature peak is assigned to the reduction of CuO crystallites [60].

The existence of vacancies on the surface of the support is a vital factor in achieving dispersion of ionic species [61]. Cu^{+2} species can be located at surface vacancies of ZrO_2 leading to a high dispersion of copper. These species are responsible for the low temperature reduction peaks. Previous work reports a dispersion capacity of 8.6 ions of Cu^{+2} per nm^2 of ZrO_2 . Loads of copper species higher than this dispersion capacity of ZrO_2 will result in the formation of Cu^{+2} ions being gradually surrounded by other Cu^{+2} ions forming CuO bulk species leading to an increase of the reduction temperature of these species [58]. Bulk CuO exhibits a broad TPR peak at ca. 300°C (Fig. 5).

γ - Al_2O_3 is also able to stabilize Cu^{+2} due to the existence of tetrahedral and octahedral vacancies on its surface [62], while SiO_2 is not able due to its structurally saturated surface. Previous work [63] reported the formation of bulk CuO modulated in terms of the ratio Cu/SSA or “copper charge/specific support area (SSA)” of 4.5 atoms of Cu per nm^2 of ZrO_2 support. Considering that the ZrO_2 used in our work has a specific surface area of $146 \text{ m}^2 \text{ g}^{-1}$ the appearance of bulk CuO would occur approximately in copper charges of 7 wt.%. In

addition, considering that the γ -Al₂O₃ used in our work has a specific surface area of 212 m² g⁻¹ it can be expected that the formation of CuO species would begin to appear with copper loading close to 10 wt.%. The detection of CuO bulk species in the XRD profiles (Fig. 2) is somewhat difficult.

Dispersion on metallic copper and the specific copper surfaces of the catalysts were determined by chemisorption of N₂O. Cu/ZrO₂ shows the highest dispersion with 38% and the largest metallic surface area of Cu⁰ (Table 4). Although ZrO₂ has the smallest specific surface it is able to disperse substantial amount of impregnated copper species due to the strong interaction between copper species and support [64]. Cu/SiO₂ shows a significantly lower copper dispersion and specific copper surface of the catalysts which are more likely due to a more intense sintering of copper particles.

Table 4. Catalysts characterization by N₂O chemisorption

Parameter	Catalyst		
	5%Cu/SiO ₂	5%Cu/ γ -Al ₂ O ₃	5%Cu/ZrO ₂
N ₂ O (μ mol N ₂ O g _{cat} ⁻¹)	203	277	301
Dispersion (%)	26	35	38

XPS parameters from the reduced copper catalysts are summarized in Table 5 and Fig. 6.

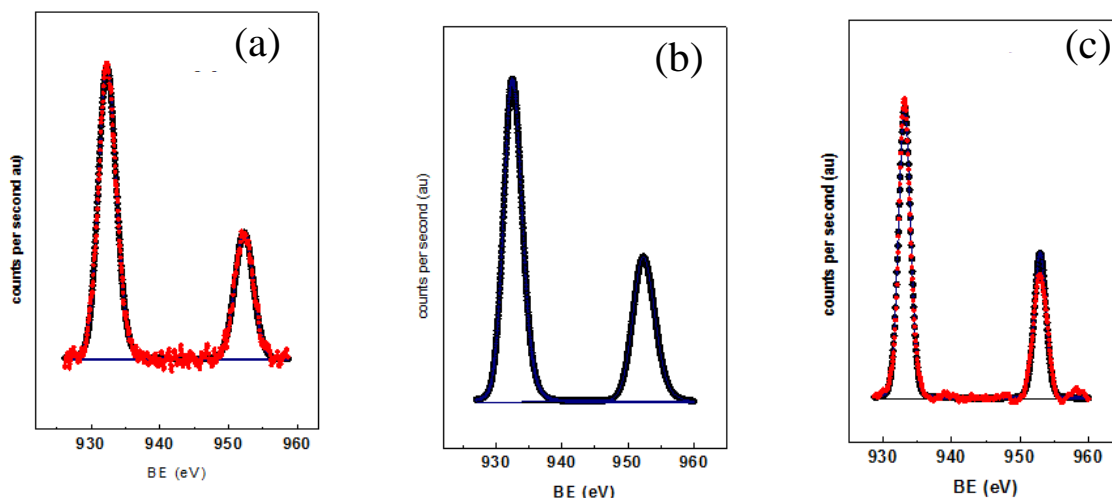


Fig. 6. XPS of (a) 5%Cu/SiO₂, (b) 5%Cu/Al₂O₃ and (c) 5%Cu/ZrO₂.

All reduced catalysts exhibited symmetrical Cu3p_{3/2} and Cu2p_{1/2} peaks with binding energies between 932.5 and 952.4 eV respectively. A satellite was not detected at approximately 942 eV suggesting absence of Cu⁺² species [65]. Because the binding energies of Cu⁰ and Cu⁺ are similar it is difficult to differentiate them based only on Cu3p_{3/2}, so we used the modified Auger parameter (α Cu) for further conclusions.

Table 5. Binding energies (eV) of internal levels, Auger parameter and atomic ratios of supported copper catalysts

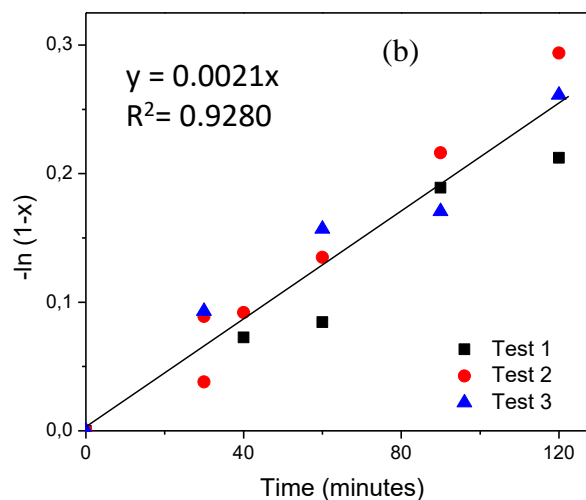
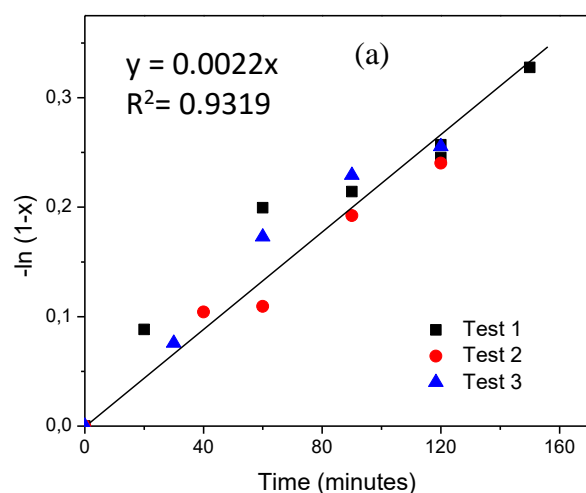
Catalyst	Cu2p _{3/2}	M2p or M3d	α Cu (Auger)	Cu/M ^a atomic ratio
5%Cu/ZrO ₂	932.5	182.2	1850.9	0.016
5%Cu/Al ₂ O ₃	932.5	74.5	1851.0	0.021
5%Cu/SiO ₂	932.4	103.4	1850.8	0.027

The value of αCu at approximately 1851.0 eV for reduced copper catalysts suggests that the copper species may prevail on the catalyst surface as Cu° . The value of the atomic surface ratio Cu/M (M=Al, Si, Zr) determined via XPS for the reduced samples increases in the following order: $\text{Cu/ZrO}_2 < \text{Cu}/\gamma\text{-Al}_2\text{O}_3 < \text{Cu/SiO}_2$. The difference in the distribution of copper species on each support can be tentatively identified with the Cu/M surface atomic ratio value. In this case, a lower Cu/M suggests a more homogeneous distribution of copper species on ZrO_2 support in agreement with the aforementioned results via XRD (Fig. 2), TPR (Fig. 5), chemisorption of N_2O (Table 4).

3.2 Catalytic activity

Glycerol conversion profile in the first 120 minutes of reaction was used to determine the kinetic parameters such as the reaction order (n) and the apparent kinetic constant (k) values expressed in terms of $\text{min}^{-1} \text{m}_{\text{cat}}^{-2}$. The first 120 minutes have been studied in order to ensure the evaluation of the catalytic performance under conditions where the reaction is kinetically controlled and there is a minimization of the influence of possible product-catalyst interaction. Moreover, for the determination of the kinetic constant an isothermal process; constant volume of the reaction medium and absence of mass transfer effect have been considered. The Weisz-Prater (WP) criterion was used to verify the absence of intraparticle diffusion limitation as well as the assumption of spherical particles and the consideration of an apparent first order reaction. It was obtained a value of WP of 0.12 in the worst scenario. WP values less than 0.3 ensure that there is no mass transfer, thus our system meets the WP criteria. After 2 hours of reaction the conversion observed for 5%Cu/ ZrO_2 , 5%Cu/ Al_2O_3 and 5%Cu/ SiO_2 catalysts were at about 30%, 25% and 22%, respectively.

In the present study the activity results were expressed in terms of conversion (X). The same catalytic test was performed multiple times to check the reproducibility. The results are presented in Fig. 7 with the plot of $-\ln(1-X)$ versus *time* to demonstrate an apparent kinetic of an irreversible first order reaction with a constant density system. A straight line passing through the origin was obtained (Fig. 7) where the corresponding slope is equal to the apparent kinetic constant of each catalyst. It was represented the results from the repeated experiments for each catalyst in the corresponding plot. The highest kinetic constant was found for the 5%Cu/ZrO₂ catalyst.



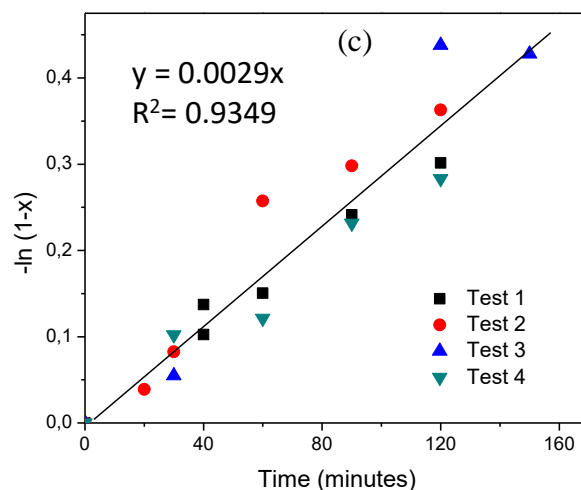


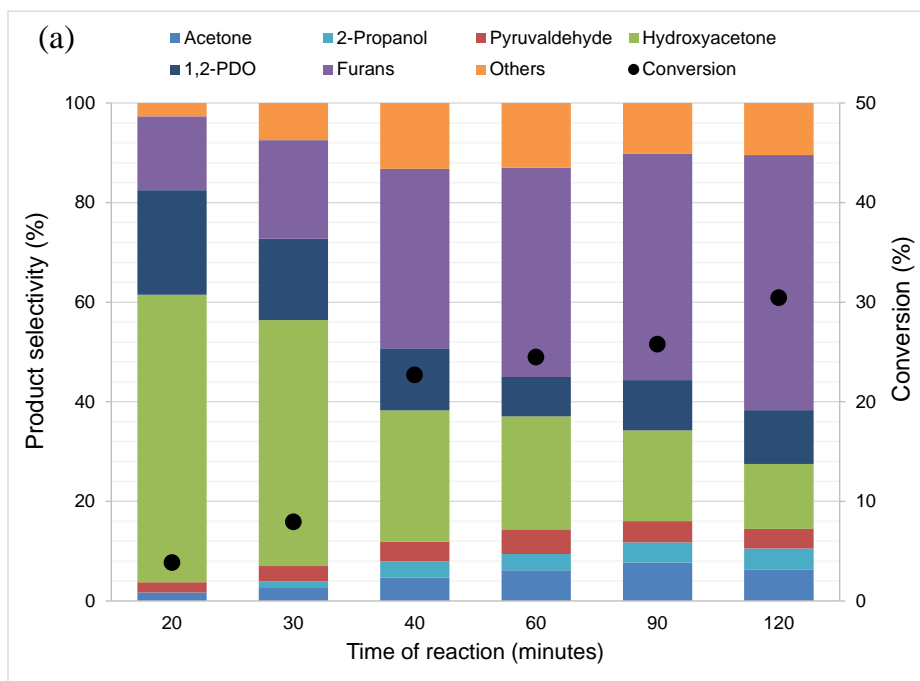
Fig. 7. Reaction demonstrating an apparent first order kinetic (a) 5%Cu/SiO₂, (b) 5%Cu/Al₂O₃ and (c) 5%Cu/ZrO₂.

The physical-chemical properties of the support have vital influence on the dispersion of metallic copper species influencing the catalytic performance as noticed in Table 6, which represents the relationship of the kinetic constants expressed in $\mu\text{mol m}_{\text{cat}}^{-2}$ with the total quantity of N₂O chemisorbed ($\mu\text{mol m}_{\text{cat}}^{-2}$). Table 6 also shows the relationship of the corresponding kinetic constants to the total acidic sites expressed in ($\mu\text{mol m}_{\text{cat}}^{-2}$). Thus, an increase in the apparent kinetic constant with both total quantity of N₂O chemisorbed and the total quantity of acidic sites was observed.

Table 6. Apparent kinetic constant of the copper catalysts

Apparent first order kinetic constant, k	5%Cu/SiO ₂	5%Cu/ γ -Al ₂ O ₃	5%Cu/ZrO ₂
k (min ⁻¹)	0.0022	0.0021	0.0029
k (min ⁻¹ m _{cat} ⁻²)	4.5×10 ⁻⁶	5.8×10 ⁻⁶	1.1×10 ⁻⁵

Under the experimental conditions, a negligible conversion of glycerol and hydroxyacetone selectivity were observed when the supports were directly used as catalysts in the activity tests. Fig. 8 shows their catalytic performance monitored in different times of reaction. Cu/ZrO₂ catalyst (Fig. 8a) shows a glycerol conversion of at about 4% at 20 minutes reaching at about 30% of conversion at 120 minutes of reaction. Cu/ γ -Al₂O₃ (Fig. 8b) exhibits a glycerol conversion between 8 to 25% in the range of 120 minutes of reaction. In the case of Cu/SiO₂ catalyst (Fig. 8c) it is observed a glycerol conversion of 8% at 20 minutes of reaction and at about 20% of conversion at 120 minutes of reaction.



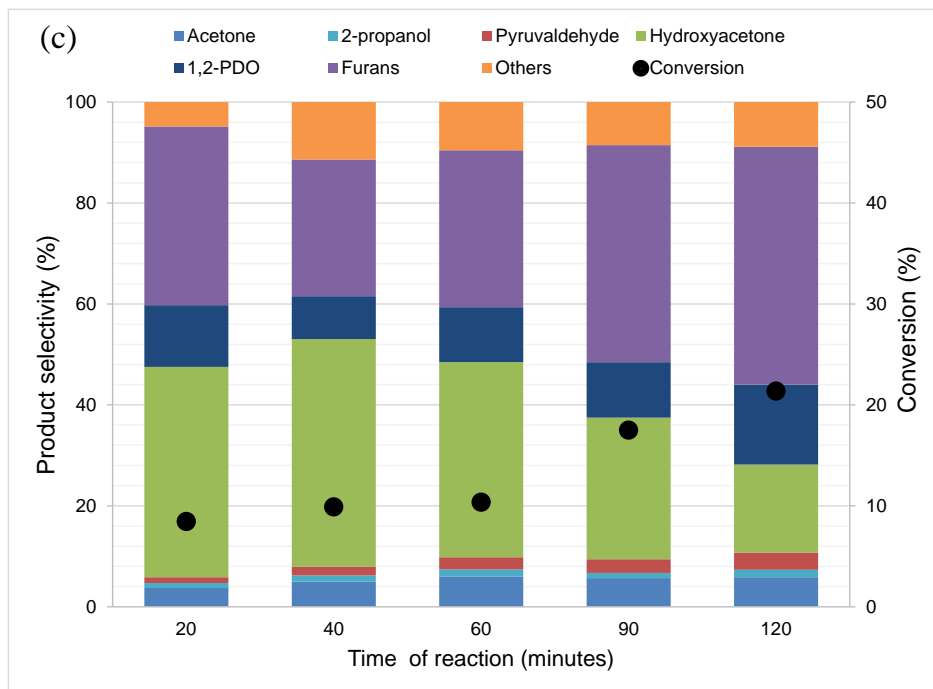
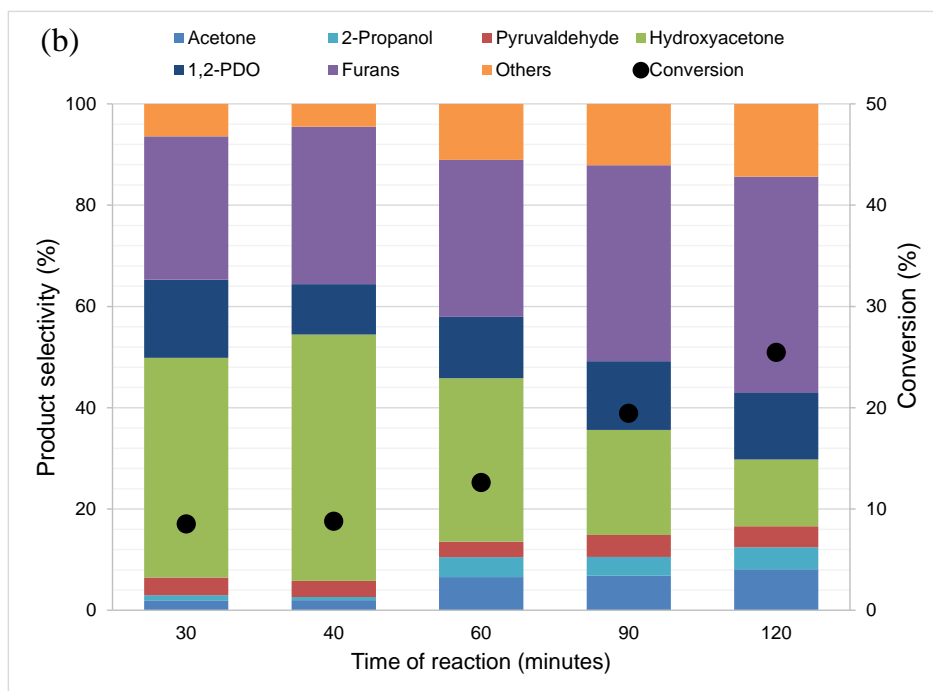


Figure 8. Catalytic performance of copper based catalysts. (a) 5% Cu/ZrO₂, (b) 5% Cu/Al₂O₃ and (c) 5% Cu/SiO₂.

The main products observed in the reaction was acetone, 2-propanol, pyruvaldehyde, hydroxyacetone, 1,2-propanediol, furan derivatives and other unidentified compounds possibly produced by secondary reactions between the compounds in the reaction mixture. It is noticed for the copper catalysts that the highest selectivity towards hydroxyacetone was in first minutes of reaction. In this respect, hydroxyacetone selectivity of 57% and 41% was observed respectively for Cu/ZrO₂ and Cu/SiO₂ catalysts at 20 minutes of reaction, whereas for Cu/ γ -Al₂O₃ sample a hydroxyacetone selectivity of 43% was noticed at 30 minutes of reaction. Previous work [9] reported over Cu-Al (50:50) catalyst prepared by coprecipitation a hydroxyacetone selectivity of 92% and 24% of glycerol conversion at 493 K in aqueous medium under N₂ atmosphere in autogenous condition. W. Suprun *et al.* [66] reported hydroxyacetone selectivity of 23% and 100% of conversion in the dehydration of glycerol over Al₂O₃-PO₄ catalyst at 280⁰C. Chiu et al.[16] reported that copper-chromite catalyzes the dehydration of glycerol with a selectivity towards hydroxyacetone of 70% and 22% of glycerol conversion.

Hydroxyacetone was the major product observed in the initial reaction period as shown Fig. 9. In addition, the highest yield towards hydroxyacetone was noticed for 5%Cu/ZrO₂. Hydroxyl terminal groups of the glycerol molecule interacting with the Lewis acid sites on the catalyst surface may promote the formation of an enol intermediate which rapidly reorganizes to form hydroxyacetone. Thus, hydroxyacetone can be obtained by direct dehydration of glycerol followed by a keto-enolic tautomerization [67]. Pyruvaldehyde was also observed and it can be formed from hydroxyacetone dehydrogenation.

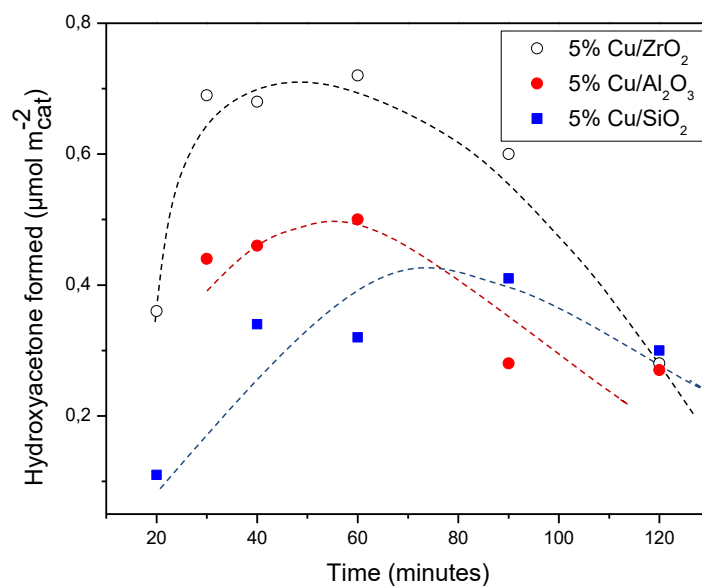
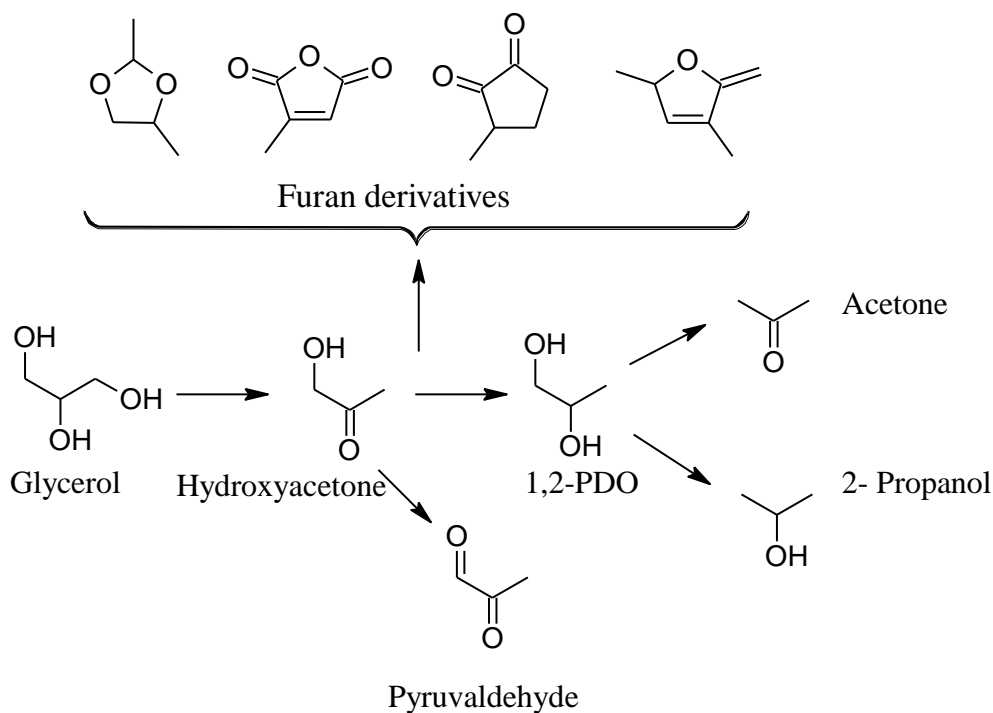


Fig. 9. Glycerol conversion towards hydroxyacetone. (Dashed lines only serve to guide the eyes).

After 120 minutes of reaction, acetone, 2-propanol and furan derivatives were also observed. These products were formed from the degradation of hydroxyacetone. Earlier works report that hydroxyacetone is converted to carboxylic acids which allow acetone to be formed via ketonization. Catalytic cyclisation to form furan derivatives are also observed. It must be added that 1,2 propanediol (1,2-PDO) was also detected. Previous work [9] reported that glycerol hydrogenolysis to 1,2-PDO proceeds through a dehydrogenation-dehydration-hydrogenation mechanism. In that case hydroxyacetone is the intermediate to 1,2-PDO. Copper may serve as active sites for the subsequent hydrogenation step to 1,2-PDO by the formation of active hydrogen atom originating from the dehydrogenation step. The general chemical route based on the main products detected by gas chromatograph and mass spectrometry is shown in Scheme 1.



Scheme 1. Identified products in the glycerol dehydration.

3.3 Catalyst Recycling

The recycling of 5%Cu/ZrO₂ catalyst during the selective conversion of glycerol to hydroxyacetone was investigated. After the first test (Postcycle 1), the catalyst was recovered by decantation and it was washed with a 50/50 mixture methanol-water and dried at 100°C. The dried catalysts were calcined at 400 °C for 4 hours and finally reduced at 400 °C for 4 hours under hydrogen flow. The resultant reduced catalyst was used for the next cycle (Postcycle 2) under conditions that allowed to maintain the same glycerol/catalyst molar ratio used in the cycle 1. The same process of separation, washing and reactivation of the catalyst has been implemented for the Postcycle 3. As shown Fig. 10 the fresh 5%Cu/ZrO₂ gives at about 30% of glycerol conversion at 120 minutes of reaction. During the Postcycle 2 the

conversion of glycerol decreased to about 10% and in the third cycle the conversion decreased to reach at about 5%.

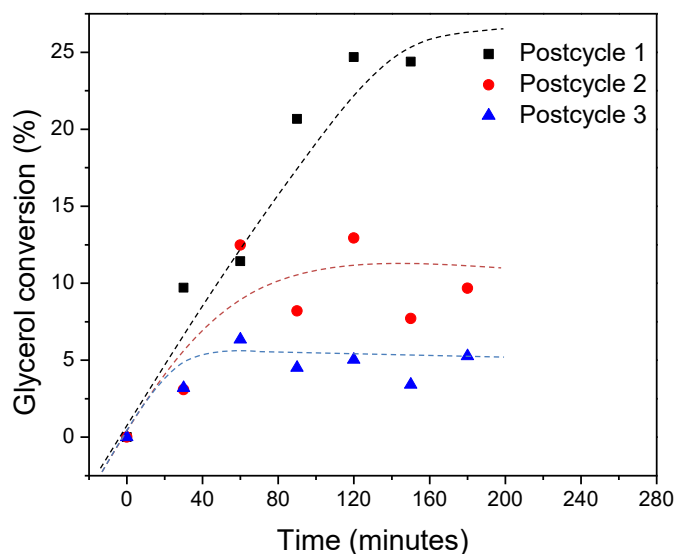


Fig. 10. 5%Cu/ZrO₂ catalyst recycling process in the glycerol dehydration. (Dashed lines only serve to guide the eyes).

To identify the origin of the deactivation, the fresh and used 5% Cu/ZrO₂ catalysts (reactivated by calcination-reduction) were characterized by nitrogen physisorption (Fig. S1 and Table 7) and N₂O chemisorption (Fig. S2 and Table 7). In addition, X-ray diffraction (Fig. S3) and scanning electron microscopy coupled to an energy dispersive X-ray spectrometer (SEM-EDS) (Table 7) were performed. The EDS results indicate that copper species are homogeneously distributed over ZrO₂ and there is no appreciable variation in the atomic relationship Cu/Zr after each recycling (Table 7).

Table 7. Properties of the 5%Cu/ZrO₂ catalyst during the recycling process

Sample	S _{BET} (m ² g ⁻¹)	V _P (cm ³ g ⁻¹)	d _p (nm)	N ₂ O (μmol N ₂ O g _{cat} ⁻¹)	Cu/Zr ^a
Fresh	131	0.13	4.01	301	0.075
Postcycle 1	128	0.15	4.24	286	0.090
Postcycle 2	129	0.15	4.55	164	0.075
Postcycle 3	116	0.14	4.86	170	0.079

^a EDS

Change of the textural properties of 5%Cu/ZrO₂ material in the recycling was negligible (Table 7). The total amount of chemisorbed N₂O was progressively reduced between each cycle (Fig. S2 and Table 7). Moreover, the X-ray diffraction of the used materials after each reactivation indicates some sintering of copper species by the appearance of copper oxide phase (Fig. S3). The observed sintering of copper particles after the catalytic cycles may result in the loss of active site which can be considered as the main factor contributing to the observed catalyst deactivation.

3.4 DFT study

To gain molecular insights and explain the support effects, adsorption energies of glycerol, and hydroxyacetone were computed using DFT calculations. The effect of hydroxylation on Al₂O₃ and ZrO₂ supports due to water dissociation, which is also related to Brönsted acid site were also investigated. Three possible adsorption sites were considered on each surface i.e. Cu site, Al or Zr site on support and interface site between Cu cluster and support. Here, we

report only adsorption at the most stable one. The adsorption energies were calculated using equation (9) and summarized in Table 8.

$$E_{ad} = E_{total} - E_{clean\ surface} - E_{adsorbate} \quad (9)$$

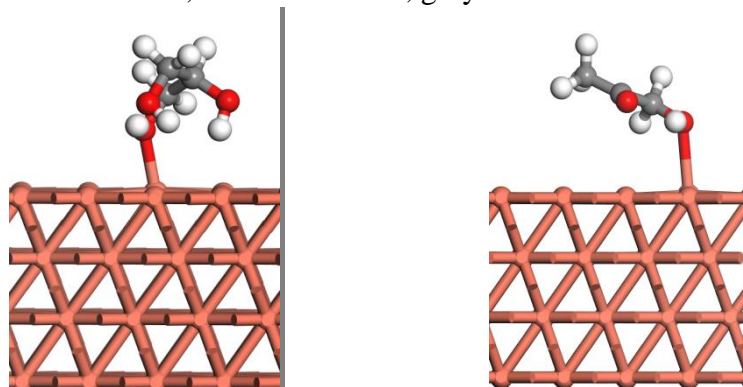
where E_{ad} is adsorption energy, E_{total} is energy of structures with glycerol/hydroxyacetone adsorption, $E_{clean\ surface}$ is energy of structures without glycerol/hydroxyacetone adsorption and $E_{adsorbate}$ is energy of isolated glycerol/hydroxyacetone molecule. The more negative values of E_{ad} , the stronger adsorption.

Table 8. Adsorption energies (kJ mol^{-1}) of glycerol and hydroxyacetone on Cu(111), $\text{Cu}_{13}/\text{Al}_2\text{O}_3(110)$, $\text{Cu}_{13}/\text{ZrO}_2(111)$, $\text{Cu}_{13}/\text{hydroxylated Al}_2\text{O}_3(110)$, and $\text{Cu}_{13}/\text{hydroxylated ZrO}_2(111)$ surfaces and Bader charge analysis of Cu_{13} cluster. The corresponding adsorption structures are shown in Fig. 11.

	Adsorption energy (kJ mol^{-1})		Charge of Cu_{13} cluster (e^-)
	glycerol	hydroxyacetone	
Cu(111)	-100.12	-102.13	
$\text{Cu}_{13}/\text{Al}_2\text{O}_3(110)$	-337.77	-252.71	+0.13
$\text{Cu}_{13}/\text{hydroxylated Al}_2\text{O}_3(110)$	-337.86	-274.01	+0.55
$\text{Cu}_{13}/\text{ZrO}_2(111)$	-151.04	-178.36	-0.28
$\text{Cu}_{13}/\text{hydroxylated ZrO}_2(111)$	-127.78	-159.66	-0.51

618 (a) Cu(111)

619 Orange atoms are Cu, red atoms are O, grey atoms are C and white atoms are H.

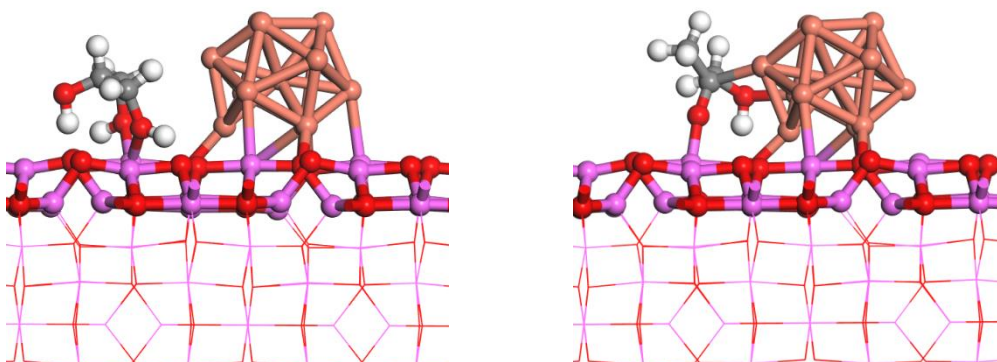


620

621

622 (b) Cu₁₃/Al₂O₃(110)

623 Purple atoms are Al.

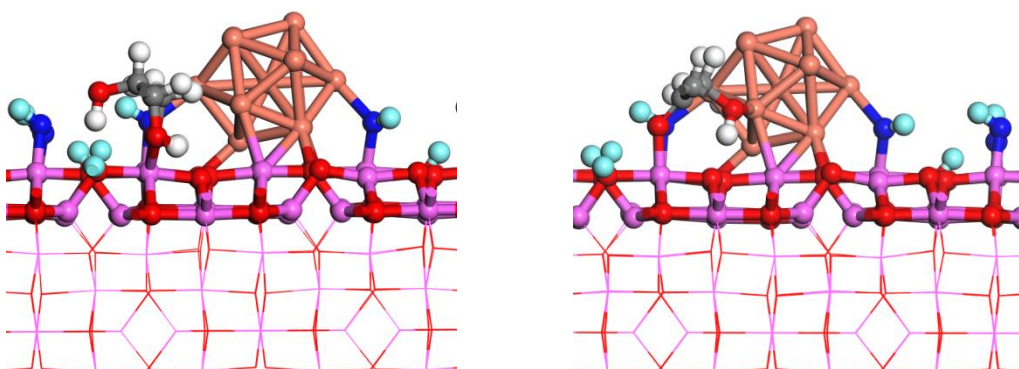


624

625

626 (c) Cu₁₃/hydroxylated Al₂O₃(110)

627 Blue atoms and light green atoms are O and H from hydroxylation, respectively.

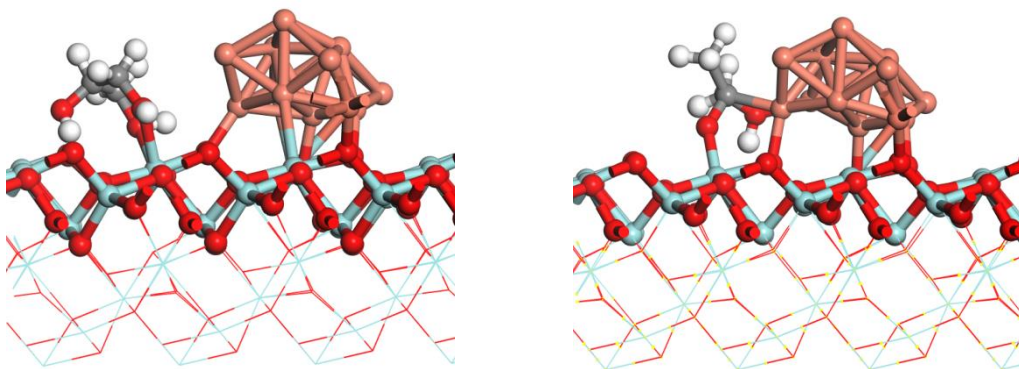


628

629

630 (d) Cu₁₃/ZrO₂(111)

631 Light green atoms are Zr.



(e) $\text{Cu}_{13}/\text{hydroxylated ZrO}_2(111)$

Blue atoms and dark green atoms are O and H from hydroxylation, respectively.

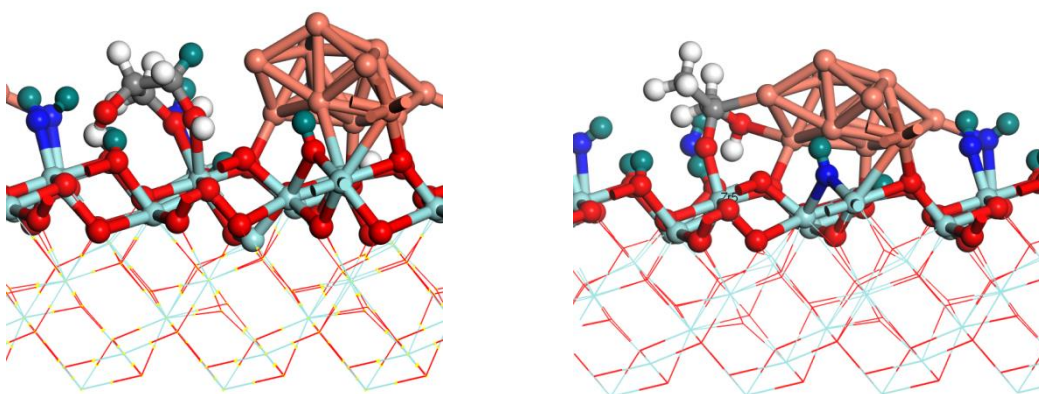


Fig. 11. Most stable adsorption structures of glycerol (left) and hydroxyacetone (right) on (a) $\text{Cu}(111)$, (b) $\text{Cu}_{13}/\text{Al}_2\text{O}_3(110)$, (c) $\text{Cu}_{13}/\text{hydroxylated Al}_2\text{O}_3(110)$, (d) $\text{Cu}_{13}/\text{ZrO}_2(111)$, and (e) $\text{Cu}_{13}/\text{hydroxylated ZrO}_2(111)$ surfaces.

Glycerol and hydroxyacetone adsorption strength are in the order of $\text{Cu}(111) < \text{Cu}_{13}/\text{ZrO}_2(111) < \text{Cu}_{13}/\text{Al}_2\text{O}_3(110)$. The relatively strong adsorption indicates that the support significantly facilitate interaction with glycerol and hydroxyacetone. The strong glycerol adsorption on $\text{Cu}_{13}/\text{Al}_2\text{O}_3(110)$ and $\text{Cu}_{13}/\text{ZrO}_2(111)$ surfaces could result from bidentate binding that both oxygen ends of glycerol molecule bond to the same metal atom

of support (Al or Zr) whereas monodentate binding occurs on Cu(111) surface (Fig. 11, left). Hydroxyacetone prefers to bind through oxygen atom of hydroxyl group on Cu(111) surface while it binds at the interface site where oxygen of carbonyl group interacts with metal site of support and oxygen of hydroxyl group interacts with copper site (Fig. 11, right). Thus, hydroxyacetone interaction on $\text{Cu}_{13}/\text{Al}_2\text{O}_3(110)$ and $\text{Cu}_{13}/\text{ZrO}_2(111)$ surfaces is significantly stronger than that on Cu(111) surface. As illustrated in Fig. 11, glycerol favours to adsorb at support's metal atom site locating adjacent to the Cu cluster and hydroxyacetone prefers to adsorb at the interface site requiring both support's metal atom site and Cu site. This suggests the vital synergistic role of the interface Cu-support as the active site and the significance of high copper particles dispersion, in which turn the increase of interfacial Cu-support sites. Hydroxylation on $\text{Cu}_{13}/\text{Al}_2\text{O}_3(110)$ and $\text{Cu}_{13}/\text{ZrO}_2(111)$ surfaces induce different impact on binding strength. Hydroxylation on $\text{Cu}_{13}/\text{Al}_2\text{O}_3(110)$ facilitates hydroxyacetone adsorption to be stronger while it weakens glycerol and hydroxyacetone adsorption on $\text{Cu}_{13}/\text{ZrO}_2(111)$, yet the favourable adsorption site and adsorption characteristic (monodentate/bidentate) are similar to those without hydroxylation. Furthermore, Bader charge analysis (Table 8) of Cu_{13} cluster was performed to better understand the effect of support. Cu_{13} supported on Al_2O_3 lose electrons to Al_2O_3 showing positive charge while Cu_{13} supported on ZrO_2 gain electrons from ZrO_2 showing negative charge. It is implied that ZrO_2 support shows stronger acidity compared to Al_2O_3 support. The hydroxylation increases the degree of electrons transfer from Cu_{13} cluster to Al_2O_3 and from ZrO_2 to Cu_{13} cluster resulting in higher positive charges of supported Cu_{13} on Al_2O_3 and higher negative charge of supported Cu_{13} on ZrO_2 .

4. Discussion

To establish relationships between activity and structural parameters the copper based catalysts were evaluated in the glycerol dehydration. Fig. 12 illustrates a plot correlating the produced hydroxyacetone expressed in terms of $\mu\text{mol m}_{\text{cat}}^{-2}$ at 20% of conversion with the total number of exposed metallic copper species expressed in terms of the total quantity of chemisorbed N_2O ($Y_{\text{N}_2\text{O}}$, $\mu\text{mol N}_2\text{O m}_{\text{cat}}^{-2}$) and with the total number of acid sites of the catalysts expressed in terms of $\mu\text{mol NH}_3 \text{ m}_{\text{cat}}^{-2}$.

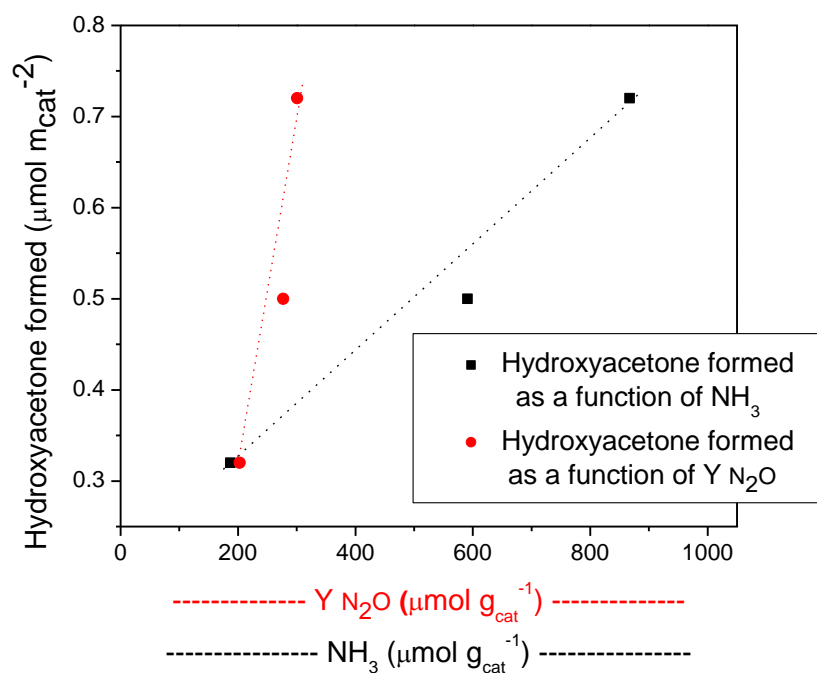


Fig. 12. Relationship between the total quantity of the produced hydroxyacetone versus exposed metallic copper atoms and the total quantity of acidic sites. (Dashed lines only serve to guide the eyes).

In the formation of hydroxyacetone stands out a lower sensitivity to the total number of acidic sites compared to the total number of exposed copper atoms which is reflected in the quantity of chemisorbed N_2O . A lower quantity of chemisorbed N_2O exhibits a higher hydroxyacetone yield when compared with the same quantity of acidic sites ($\mu\text{mol NH}_3 \text{ m}_{\text{cat}}^{-2}$).

The calculation results also reveal that hydroxyacetone and glycerol bind stronger on $\text{Cu}_{13}/\text{Al}_2\text{O}_3(110)$, $\text{Cu}_{13}/\text{ZrO}_2(111)$ surfaces compared to $\text{Cu}(111)$ surface. Also, glycerol is favourable to adsorb at support metal site close to copper cluster and hydroxyacetone is favourable to adsorb at the interface copper-support site (Fig. 11 (right)). These results suggest the synergistic role of acid sites (Al or Zr) of supports and copper cluster to promote hydroxyacetone and glycerol interaction with surfaces. In addition, the active role of the interfacial sites suggests the positive effects of highly dispersed Cu over support on catalytic reactivity. The DFT calculations also indicate that stronger acidity of ZrO_2 may better promote moderate interaction with intermediates while relatively weak acidity of Al_2O_3 results in too strong interaction with intermediates. Furthermore, the negative charges of supported Cu cluster on ZrO_2 may indicate the number of acid sites increase with copper introduction on ZrO_2 support.

It should be added that the highest kinetic constant indicates that the most active catalyst is the 5%Cu/ ZrO_2 catalyst. Particularly, ZrO_2 has been described as a preventive element for sintering copper species and it is therefore considered to be a structural promoter [68]. It is important to complement that the results of TPR indicate that the presence of ZrO_2 facilitates the reduction of copper species, as well as the results of XRD, N_2O chemisorption, EDS and

XPS which suggest that ZrO_2 support leads to a homogeneous distribution of copper species and higher dispersion of the copper species compared with $\gamma\text{-Al}_2\text{O}_3$ and SiO_2 . In addition, pyridine infrared indicates that 5%Cu/ ZrO_2 and 5%Cu/ $\gamma\text{-Al}_2\text{O}_3$ catalysts present both acidic sites of Lewis and Brönsted. For 5%Cu/ SiO_2 only Lewis acid sites were found.

5. Conclusions

The dehydration reaction of glycerol to hydroxyacetone on copper based catalysts suggests apparent first order kinetics. By NH_3 -TPD, it has been observed that the 5%Cu/ ZrO_2 exhibited the highest total quantity of acidic sites and total amount of N_2O chemisorbed suggesting higher dispersion of copper species compared with 5%Cu/ $\gamma\text{-Al}_2\text{O}_3$ and 5%Cu/ SiO_2 catalysts. XRD analysis suggests that copper species are finely dispersed on the support. XPS analysis identified that copper species are found in metallic state at the catalyst surface and the atomic ratio (Cu/M) (M= Si, Al or Zr) suggests that copper species are more homogeneously distributed on ZrO_2 surface.

Complementary study of DFT indicates that both glycerol and hydroxyacetone adsorb significantly stronger on $\text{Cu}_{13}/\gamma\text{-Al}_2\text{O}_3$ (110) and $\text{Cu}_{13}/\text{ZrO}_2$ (111) compared to Cu (111) which further suggests that the active sites for glycerol and hydroxyacetone adsorption are the metal support site and the dual site consisting of Al or Zr of the support (ZrO_2 and $\gamma\text{-Al}_2\text{O}_3$) of the copper species.

The kinetic constants expressed in $\mu\text{mol m}_{\text{cat}}^{-2}$ indicate that the most active material for glycerol dehydration has been the 5%Cu/ZrO₂ catalyst. A linear correlation between the yield of hydroxyacetone expressed in terms of $\mu\text{mol m}_{\text{cat}}^{-2}$ with the total quantity of chemisorbed N₂O and the total quantity of acidic sites suggest that the copper dispersion is a sensitivity factor for the activity in the glycerol dehydration.

The sintering of copper particles between each catalyst recycling step by the thermal activation process (calcination-reduction) is the main descriptor responsible for the lost in the activity for the 5%Cu/ZrO₂ in the recycling study in agreement with the progressive decrease in the total quantity of N₂O chemisorbed after each cycle. In addition, the characterization by EDS did not indicate appreciable variation in the atomic Cu/Zr ratio between each one of the reactions in the recycling process.

Acknowledgements

The authors are grateful to FONDECYT 1201936 and FONDECYT 1180243 for the financial support. P.H would like to thank computational resources from NSTDA Supercomputer Center (ThaiSC) and National Nanotechnology Center (NANOTEC).

References

- [1] S. Sato, M. Akiyama, R. Takahashi, T. Hara, K. Inui, M. Yokota, Appl. Catal A-Gen. 347 (2) (2008) 186-191.
- [2] A. Corma, S. Iborra, A. Velty, Chem. Rev. 107 (6) (2007) 2411-2502.

750 [3] M. Dasari, P-P. Kiatsimkul, W. Sutterlin, G. Suppes, Appl. Catal. A-Gen., 281 (1-2)
751 (2005) 225-231.

752 [4] J. Shabaker, G. Huber, J. Dumesic, J. Catal., 222 (1) (2004) 180-191.

753 [5] A. Corma, G. Huber, L. Sauvanaud, P. O'Connor, J. Catal. 247 (2), (2007) 307-327.

754 [6] S. Demirel, K. Lehnert, M. Lucas, P. Claus, Appl. Catal. B. 70 (1-4) (2007) 637-643.

755 [7] J. Barrault, Y. Pouilloux, J. Clacens, C. Vanhove, S. Bancquart, Catal. Today 75 (1-4)
756 (2002) 177-181.

757 [8] A. Corma, S. Hamid, S. Iborra, A. Velty, J.Catal. 234 (2) (2005) 340-347.

758 [9] R. Mane, A. Yamaguchi, A. Malawadkar, M. Shirai, C. Rode, RSC Adv. 3 (37) (2013)
759 16499-16508.

760 [10] M. Aresta, A. Dibenedetto, F. Nocito, C. Ferragina, J Catal. 228 (1) (2009) 106-114.

761 [11] G. Yang, Y. Ke, H. Ren, C. Liu, R. Yang, W. Dong, Chem.Eng J. 283 (2016) 759-767.

762 [12] M. Mohamad, R. Awang, W. Zin, Am. J. Appl. Sci. 8 (11) (2001) 1135-1139.

763 [13] R. Disselkamp, B. Harris, T. Hart, Catal. Commun. 9 (13) (2008) 2250-2252.

764 [14] J. Ko, I. Kim, S. Yoo, B. Min, K. Kim, C. Park, J. Bacteriol. 187 (16) (2005) 5782-5789.

765 [15] S. Sato, D. Sakai, F. Sato, Y. Yamada, Chem. Lett. 41(9) (2012) 965–966.

766 [16] C. Chiu, A. Tekeei, W. Sutterlin, J.Ronco, G. Suppes, *AIChE J.* 54 (9) (2008) 2456-
767 2463.

768 [17] A. Alhanash, E. Kozhevnikova, I. Kozhevnikov, Appl. Catal. A-Gen. 378 (1) (2010) 11-
769 18.

770 [18] S. Zhu, X. Gao, Y. Zhu, Y. Zhu , H. Zheng, Y. Li, J. Catal. 303 (2013) 70-79.

771 [19] S. Zhu, X. Gao, Y. Zhu, W. Fan, J. Wang, Y. Li, Catal. Sci. Technol. 5 (2) (2005) 1169-
772 1180.

773 [20] P. Hirunsit, C. Luadthong, K. Faungnawakij, RSC Adv. 15(5) (2015) 1118-11197.

774 [21] A. Bienholz, H. Hofmann, P. Claus, Appl. Catal. A-Gen. 391 (1-2) (2011) 153-157.

775 [22] S. Zhu, X.Gao, Y. Zhu, W. Fan, J. Wang, Y. Li, Catal. Sci. Technol. 5 (2) (2005) 1169-

776 1180.

777 [23] H. S. Fogler, Elements of Chemical Reaction Engineering, 3rd edition, Prentice Hall

778 International Series, 1988.

779 [24] O. Levenspiel, Chemical Reaction Engineering, 2nd edition, Wiley International edition,

780 1980.

781 [25] M. Digne, P. Sautet, P. Raybaud, P. Euzen, H. Toulhoat, J. Catal. 226 (2004) 54-68.

782 [26] P. Nortier, P. Fourre, A. B. M. Saad, O. Saur, J.C. Lavalley, Applied Catalysis 61 (1990)

783 141-160.

784 [27] X. Krokidis, P. Raybaud, A. E. Gobichon, B. Rebours, P. Euzen, H. Toulhoat, The

785 Journal of Physical Chemistry B 105(22) (2001) 5121-5130.

786 [28] J. P. Chou, H. Y. T. Chen, C. R. Hsing, C. M. Chang, C. Cheng, and C. M. Wei, Phys.

787 Rev. B 80 (2009) 165412.

788 [29] M. J. Piotrowski, P. Piquini, J. L. F. da Silva, Phys. Rev. B 81 (2010) 155446.

789 [30] T. T. Li, C. He, W.X. Zhang, M. Cheng, Applied Surface Science 479 (2019) 39-46.

790 [31] W. Zeng, J. Tang, P. Wang, Y. Pei, RSC Advances 6(61) (2016) 55867-55877.

791 [32] S. Chen, X. Chen, H. Zhang, Journal of Materials Science **52**(6) (2017) 3162-3168.

792 [33] H. Gao, RSC Advances, 2016. 6(105): p. 102914-102923.

793 [34] P. Hirunsit, K.-ichi Shimizu, R. Fukuda, S. Namuangruk, Y. Morikawa, M. Ehara, The

794 Journal of Physical Chemistry C 118(15) (2014) 7996-8006.

795 [35] C. H. Hu, C. Chizallet, C. M. Maury, M. C. Valero, P. Sautet, H. Toulhoat, P. Raybaud,
796 Journal of Catalysis 274 (1) (2010) 99-110.

797 [36] C. Dessal, A. Sangnier, C. Chizallet, C. Dujardin, F. Morfin, J. L. Rousset, M. Aouine,
798 M. Bugnet, P. Afanasiev, L. Piccolo, Nanoscale 11 (2019) 6897-6904.

799 [37] P. Lackner, J. Hulva, E. M. Köck, W. M. Schmölzer, J. J. Choi, S. Penner, U. Diebold,
800 F. Mittedonfer, J. Redinger, B. Klötzer, G. S. Parkinson, M. Schmid, J. Mater. Chem. A 6
801 (2018) 17587-17601.

802 [38] G. Kresse, J. Furthmüller, Computational Materials Science 6(1) (1996) 15-50.

803 [39] G. Kresse, J. Furthmüller, Physical Review B, 54(16) (1996) 11169-11186.

804 [40] J.P. Perdew, K. Burke, M. Ernzerhof, Physical Review Letters 77(18) (1996) 3865-3868.

805 [41] P.E. Blöchl, Physical Review B 50(24) (1994) 17953-17979.

806 [42] G. Kresse, D. Joubert, Physical Review B 59(3) (1999) 1758-1775.

807 [43] S. Grimme, J. Comput. Chem. 2006, 27, 1787-1799.

808 [44] S. Grimme, J. Antony, S. Ehrlich, H. Krieg, J. Chem. Phys. 2010, 132, 154104.

809 [45] C.L. Fu, K.M. Ho, Physical Review B 28(10) (1983) 5480-5486.

810 [46] H.J. Monkhorst, J.D. Pack, Phys. Rev. B, 13(12) (1976) 5188-5192.

811 [47] G. Henkelman, A. Arnaldsson, H. Jonsson, Comput. Mater. Sci. 36 (2006) 354–360.

812 [48] E. Sanville, S. D. Kenny, R. Smith, G. Henkelman, J. Comput. Chem. 2007, 28,
813 899–908.

814 [49] W. Tang, E. Sanville, G. Henkelman, J. Phys.: Condens. Matter 2009, 21, 084204

815 [50] K. Sing, Pure Appl.Chem.,54 (11), 2201-2218.

816 [51] F. López, A. Bueno, M. Illán, Appl. Catal. B-Environ. 84(3-4) (2008) 651-658.

817 [52] R. Friedman, J. Freeman, F. Lytle, J. Catal. 55 (1) (1978) 10-28.

818 [53] J. Aguado, J.M. Escola, M.C. Castro, B. Paredes, Appl Catal A Gen 284 (2005) 47–57.

819 [54] B. Chakraborty, B. Viswanathan, Catal Today 49 (1999) 253–260.

820 [55] S. E. Voltz, A. E. Hirscheler, A. Smith, J. Phys. Chem. 64 (1960) 1594.

821 [56] S. Triwahyono, T. Yamada, H. Hattori, Appl. Catal., A 2003, 242, 101-109.

822 [57] A. Gervasini, S. Bennici, Appl. Catal. A-Gen.281 (1-2) (2005) 199-205.

823 [58] Z. Liu, M. Amiridis, Y. Chen, J. Phys. Chem. B. 109 (3) (2005) 1251-1255.

824 [59] A. Y. Yin, J. W. Qu, X. Y. Guo, W. L. Dai, K. N. Fan, Appl. Catal. A, 400 (2011) 39–

825 47.

826 [60] I.C. Freitas, S. Damyanova, D.C. Oliveira, C.M.P. Marques, J.M.C Bueno, Journal of

827 Molecular Catalysis A: Chemical 381 (2014) 26-37.

828 [61] Y. Chen, L. Dong, Y. Jin, X. Bing, J. Weijie, Stud. Surf. Sci. Catal., 101, (1996) 1293-

829 1302.

830 [62] F. Severino, J. Brito, O. Carias, J. Laine, J. Catal., 102 (1) (1986) 172-179.

831 [63] G. Aguila, F. Gracia, J. Cortés, P. Araya, Appl. Catal. B-Environ. 77(3-4) (2008) 325-

832 338.

833 [64] M. Manzoli, R. Di Monte, F. Boccuzzi, S. Coluccia, J. Kaspar, Appl. Catal. B. 61 (3-4)

834 (2005) 192-205.

835 [65] S. Velu, K. Suzuki, C. Gopinath, H. Yoshida, T. Hattori, Phys. Chem. Chem. Phys. 4

836 (10) (2002) 1990-1999.

837 [66] W. Suprun, M. Lutecki, T. Haber, H. Papp, Journal Molecular Catalysis A: Chemical

838 309 (2009) 71-78.

839 [67] J. Ten Dam, U. Hanefeld, ChemSusChem 4 (10) (2011) 1017-1034.

840 [68] J. Agrell, H. Birgersson, M. Boutonnet, I. M. Cabrera, R. Navarro, J.L.G. Fierro, J. Catal.
841 219 (2) (2003) 389-403.
842
843
844
845
846
847